Characterization of Irradiated Silicon Strip Detectors Using Doping Density Simulations

A Thesis Submitted in Partial Satisfaction of the Requirements for the Degree of

BACHELOR OF SCIENCE in PHYSICS

at the

UNIVERSITY OF CALIFORNIA, SANTA CRUZ

by

R. Ford Hurley

June 2007

The thesis of R. Ford Hurley is approved by:

Professor Hartmut F.-W. Sadrozinski
Technical Advisor

Professor Clemens Heusch
Supervisor of Senior Theses 2006-2007

Professor David Belanger
Chair, Department of Physics

Abstract

Characterization of Irradiated Silicon Strip Detectors Using Doping Density Simulations

by

R. Ford Hurley

This paper will discuss the use of doping density simulation methods to study the effects of gamma and neutron irradiation on various types of silicon strip detectors. It will also discuss problems with the presented simulation method and suggest ways in which it can be improved.

Dedicated to Mary.

Acknowledgments

First of all, my family for their encouragement and support, without which I would not be in college. Chris Betancourt for teaching me how to use the lab equipment and for working so hard with me to develop the simulation method; this thesis wouldn't be at all the same without his help. Maureen Petterson for always helping me while working in the lab and for dealing with the numerous problems I ran into while doing so. Aleksander Polyakov for developing ADAP and teaching me how to use it. A big thank you is due to all of the undergrads and staff working at SCIPP that have always been available to help, talk to, or laugh with. Forest Martinez-McKinney for his help mounting and bonding detectors. And finally, my technical advisor Hartmut F.-W. Sadrozinski for his guidance, his knowledge, his curiosity, his persistence, and his sense of humor.

Contents

List of Figures

List of Tables

Chapter 1

Introduction

1.1 Silicon Strip Detectors

Silicon strip detectors (SSDs) are essentially complicated semiconductor diodes. When energetic particles pass through a diode, charge carriers are set free and cause signal pulses. Silicon detectors exploit this property in order to detect energetic particles. By adding oppositely doped silicon implants to the surface of a detector (see Figure 1.2 for a cross section), the detector is able to provide high resolution data on the path of the detected particle. As a particle moves through the depleted bulk of the detector, electron-hole pairs are created which, in the presence of an applied field, are collected at the aluminum readout strips, amplified, and sent to the readout electronics. Because of the strips, the particle's trajectory can be resolved to high resolution as it passes through the bulk. Figure 1.3 shows an illustration of this.

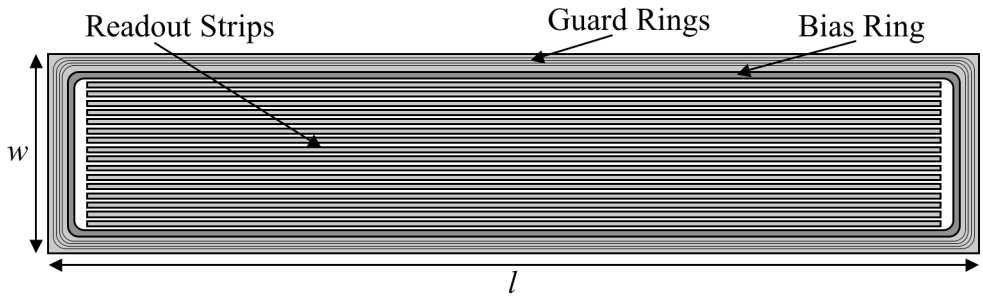

Figure 1.1: Top view of a silicon strip detector (not to scale.) Typically, $l \approx 4.7$ cm, $w \approx 0.7$ cm, and there are 32 or 64 strips.

1.2 Motivation

In the ATLAS detector at the LHC (Large Hadron Collider), silicon strip detectors will be a part of the Inner Detector and will therefore be exposed to large amounts of radiation [1]. This radiation damage changes a detector in a number of ways. One way is that the leakage current is increased, causing an increase in noise. This can be controlled by reducing the operating temperature of the detector [2]. Radiation damage also changes the effective doping density (N_{eff}) [3]. Using simulation methods, I plan to quantify this change in N_{eff} as a function of radiation fluence for different types of detectors and different types of radiation.

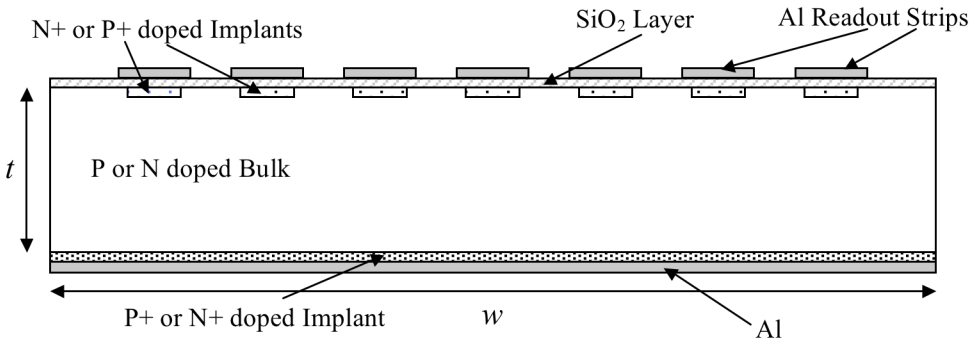

Figure 1.2: Cross section of a silicon strip detector.

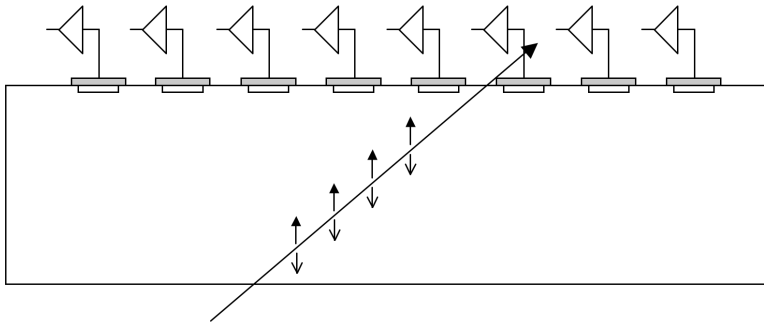

Figure 1.3: Illustration showing electron-hole pair generation from an ionizing particle. The charge carriers are collected by the Al strips and carried to the readout electronics [4].

Chapter 2

Measurements

The system we use at SCIPP for measuring capacitance-voltage (C-V) data of SSDs has been developed over the years by a number of people and is constantly being improved. One notable feature of the system is the computer program ADAP (Advanced Data Acquisition Program) developed by fellow student Aleksander Polyakov, which automates much of the process. The following is the procedure currently in use.

2.1 Procedure for Measuring C-V Data

To measure the capacitance of a detector, we mount it on a piece of G10 (a sheet of fiberglass sandwiched between copper plating) using conductive epoxy. This makes it easy to make electrical contact with the backplane of the detector. The high potential output of the LCR meter is then connected to the G10, with the low potential output connected to the bias ring on the top of the detector.

For irradiated detectors, we need to conduct these experiments at low temperature, typically -10 or -20 degrees Celsius. To accurately measure the temperature of the detector, a 100 Ω platinum thermistor (Pt100) is affixed to the G10 near the detector. The

detector is then placed inside a light-tight and thermally insulated container. To achieve the desired temperature (see Section 2.2 below) and to maintain that temperature thoughout the experiment, liquid nitrogen is periodically added to the bottom of the container. The nitrogen has the added benefit of creating a dry environment to prevent condensation on the detector.

For unirradiated detectors, the experiments were conducted at room temperature in a light-tight box. Instead of mounting the detector on G10 and attaching a bond to the bias ring, we affix the detector to a sheet of G10 with a vacuum and use probes to bias the detector. One probe makes contact with the G10 (to contact the back side of the detector) while the other is touched down to the bias ring. This is all done under a microscope with micropositioners.

The measurements are performed using two pieces of equipment: a Keithley 2410 high voltage power supply and an Agilent E4980A LCR Meter. The Keithley provides a DC bias voltage across the capacitor and measures the leakage current. The LCR superimposes an AC current onto the bias voltage and measures the capacitance and resistance of the detector, modeling it as a capacitor and a resistor in series. A schematic diagram of the low temperature experimental setup is shown in Figure 2.1.

Because we want to measure the capacitance over a large range of voltages and for a range of frequencies at each voltage, we use ADAP to control the equipment (i.e., to set voltages and frequencies) and to record the data.

For a detailed, step by step description of how to set up the experiment, please see Appendix A.

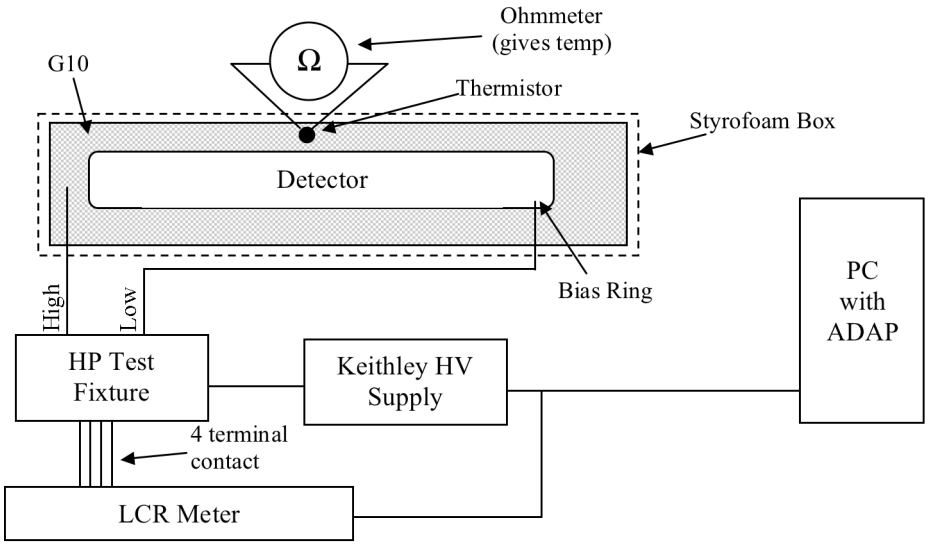

Figure 2.1: Schematic diagram of the experimental setup used to measure C-V at low temperatures.

2.2 Temperature

Irradiated detectors are extremely sensitive to temperature. The leakage current is related to the temperature by

$$I(T) \propto T^2 e^{-\frac{E_g}{2kT}} \tag{2.1}$$

where $E_g = 1.2$eV [2]. Decreasing the leakage current reduces noise and allows higher operating voltages [5]. Furthermore, self heating due to the current leads to increased temperature, which in turn leads to increased current, and so on. This is known as thermal runaway. This is why we need to periodically add nitrogen during the experiment to control the temperature. With the current system, I was able to keep the temperature constant to within 0.5°C.

Chapter 3

Simulation

To determine the doping density distribution for a given detector, we can fit a simulated C-V curve to the measured data. Figure 3.1 shows a simple approximation of how the detector depletes under reverse bias. Assuming it depletes in that way, we then make a guess for the doping density distribution and compare the simulated results to the C-V measurements. By adjusting the parameters until the simulation closely resembles the data, we can arrive at a reasonable approximation for the doping distribution.

3.1 Derivation

Beginning with Poisson's equation,

$$\frac{d^2V}{dx^2} = -\frac{\rho}{\epsilon} = -\frac{q}{\epsilon}N_{eff}(x) \tag{3.1}$$

we can calculate the electric field as a function of depletion depth.

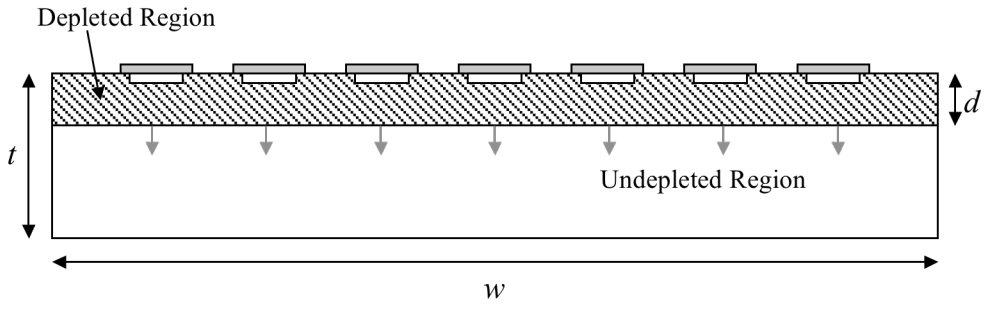

Figure 3.1: Cross section showing uniform depletion of the detector from the front side (top in this figure). As the bias voltage is increased, the depleted depth d increases.

A simple *ansatz* is to assume three different regions of constant doping densities, i.e.,

$$N_{eff}(x) = \begin{cases} N_1 & x \leq x_1 \\ N_2 & x_1 < x \leq x_2 \\ N_3 & x_2 < x \leq t \end{cases} \tag{3.2}$$

Integrating (3.1) gives,

$$E(x) = E_0 + \frac{q}{\epsilon} \int_0^x N_{eff}(x')dx' \tag{3.3}$$

Requiring the electric field to go to zero at $x = d$ produces E_0, so:

$$E(x,d) = \frac{q}{\epsilon} \left(\int_0^x N_{eff}(x')dx' - \int_0^d N_{eff}(x)dx \right) \tag{3.4}$$

Evaluating these integrals can be tricky, as they both need to be evaluated piecewise and separately over each region. For $d \leq x_1$, there is one $E(x,d)$. For $x_1 < d \leq x_2$ there are two $E(x,d)$s, one for $x \leq x_1$ and one for $x_1 < x \leq x_2$, and so on.

Figure 3.2 shows an example of the calculated electric field for 20 μm steps of d. To

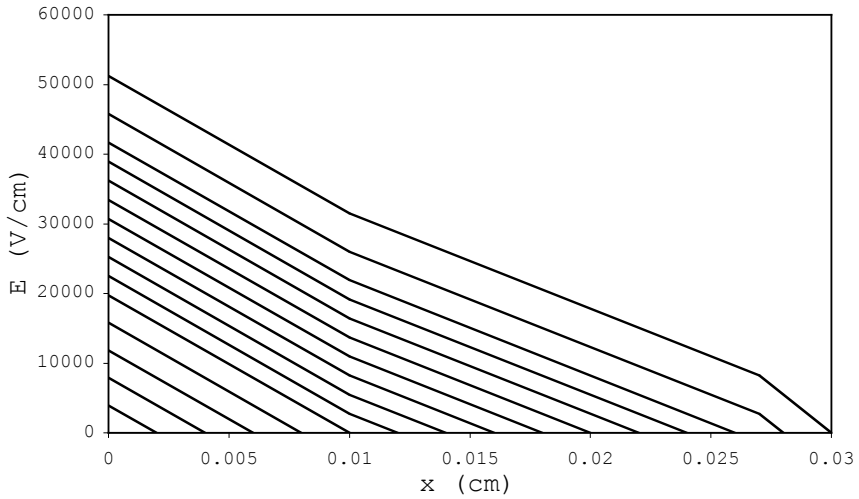

Figure 3.2: Simulated electric field at 20 μm steps of d assuming a three region doping density distribution.

find the bias voltage as a function of d, integrate $\frac{dV}{dx} = -E(x)$:

$$\int_0^d dV = V(d) - V(0) = -V(0) = V_{bias} = -\int_0^d E(x,d)dx \tag{3.5}$$

Once again, this integral needs to be evaluated carefully because of the different regions.

The capacitance of a parallel plate capacitor of thickness t and area A is given by:

$$C = \epsilon \frac{A}{t} \tag{3.6}$$

For a detector of thickness t, the capacitance as a function of depletion depth is,

$$C(d) = C_0 \frac{t}{d} \ , \tag{3.7}$$

where C_0 is the capacitance of the detector at full depletion.

Figure 3.3 shows the simulated results from integrating the electric field in Figure 3.2.

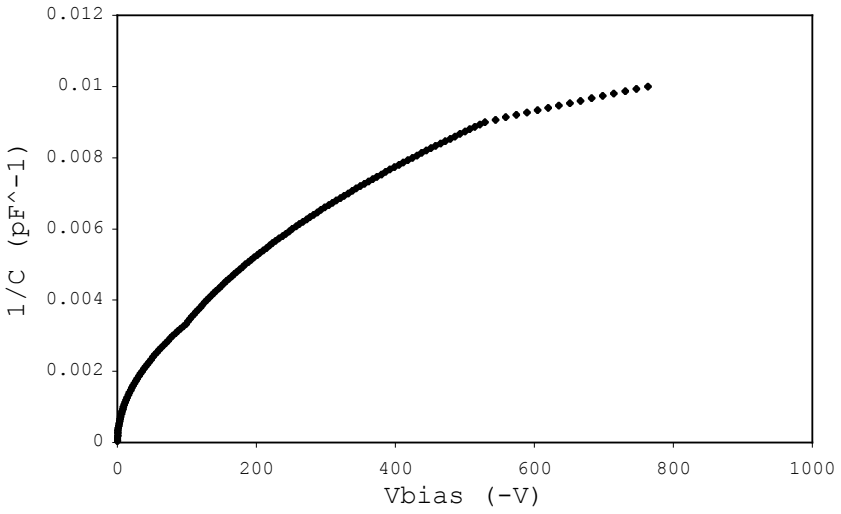

Figure 3.3: Simulated $1/C$ curve assuming a three region doping density distribution.

Plotting $1/C(d)$ versus $V_{bias}(d)$ produces a curve characteristic of silicon strip detectors. Fitting the simulated curve to the data is then simply a matter of adjusting the parameters until the two curves match up reasonably well.

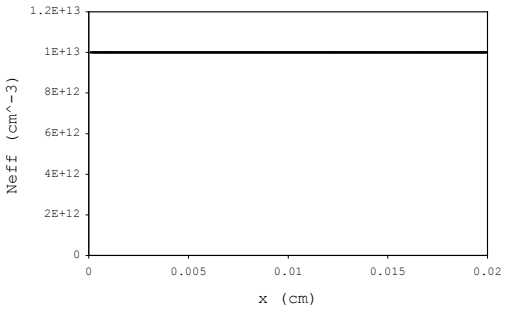

(a) $N_{eff}(x)$

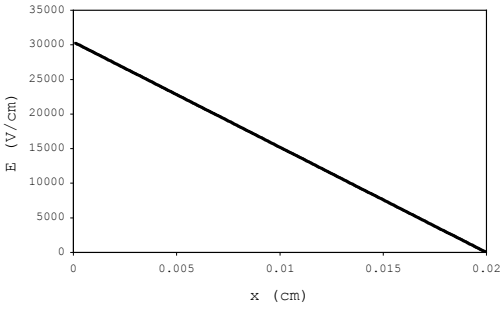

(b) $E(x)$ at depletion

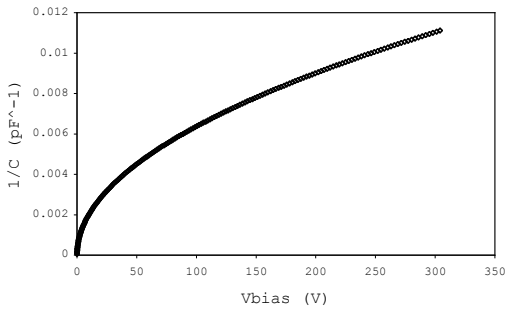

(c) $1/C$ vs. V_{bias}

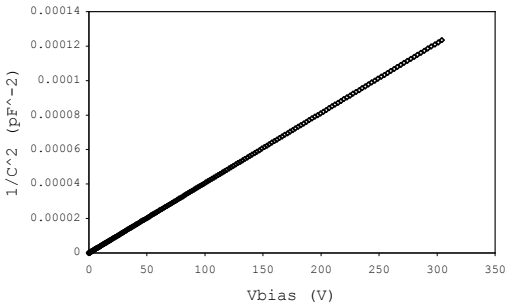

(d) $1/C^2$ vs. V_{bias}

Figure 3.4: Simulation for a 200 μm thick ideal diode.

3.2 Example Using the Ideal Diode

Applying this method to an ideal diode should yield a constant doping density, a linear electric field profile, and $1/C$ should be proportional to $\sqrt{V_{bias}}$. Evaluating 3.4 with $N_{eff}(x) = N$ gives

$$E(x, d) = \frac{qN}{\epsilon}(x - d). \tag{3.8}$$

Plugging this into 3.5 gives

$$V_{bias} = -\frac{qN}{2\epsilon}d^2. \tag{3.9}$$

Figure 3.4 shows the results of this simulation, consistent with what would be expected for an ideal diode.

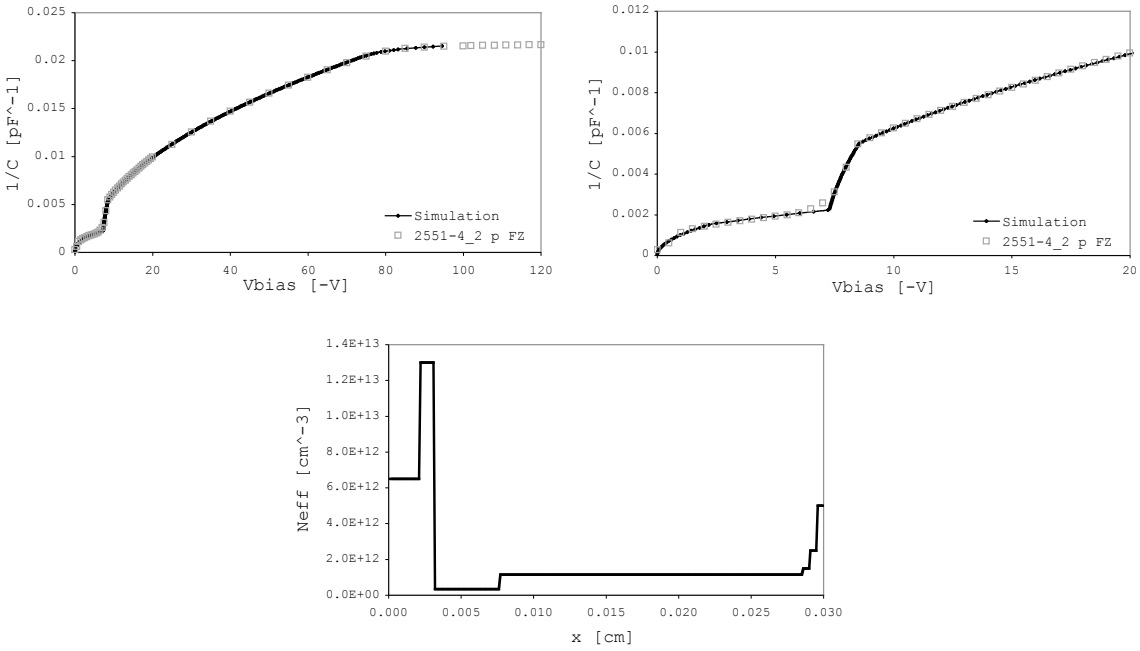

Figure 3.5: Simulated $1/C$ curve for detector 2551-4-2 (p-type FZ) showing the "foot" and extracted doping density distribution.

3.3 Problems with the Simulation

After applying this method to a few detectors, a number of problems have become apparent. First, the doping density distribution will be continuous inside a real detector, not made up of several constant regions. Still, this method produces reasonably good fits for the data.

Another problem is that some detectors may not deplete in this way at all. If a detector has undergone type inversion as a result of being irradiated, a double junction may have formed. In that case, there will be two oppositely doped regions within the detector and the depletion will not be as simple. This issue is unresolved but is beyond the scope of this paper.

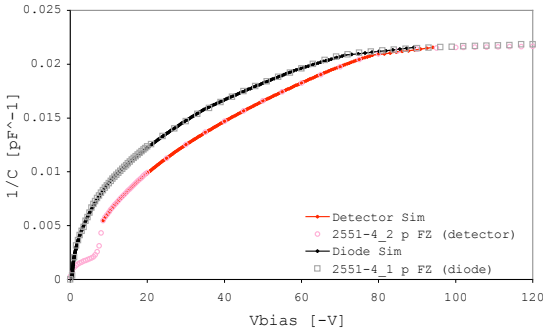

(a) $1/C$ vs. V_{bias}

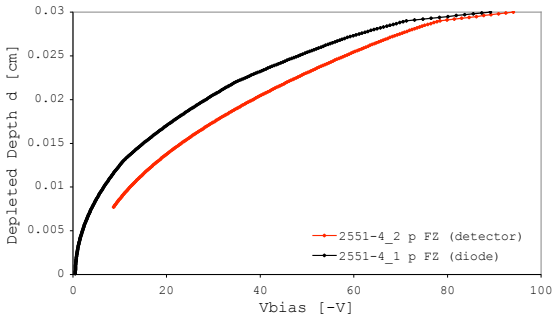

(b) Depleted Depth vs. V_{bias}

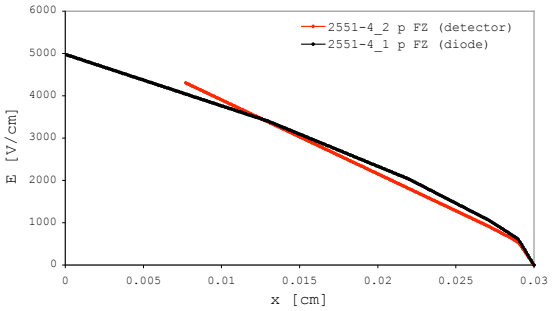

(c) Electric Field at Depletion

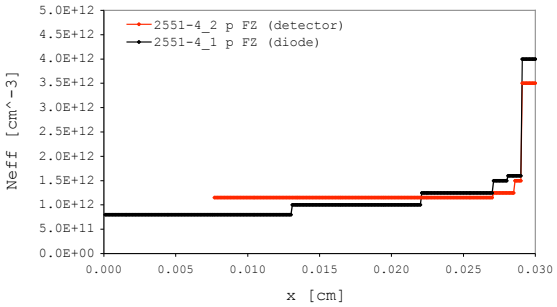

(d) $N_{eff}(x)$

Figure 3.6: Diode vs. Detector Comparison. Note the lack of the "foot" in the $1/C$ curve for the diode. The "foot" of the $1/C$ curve for the detector has been omitted from the simulation because it is not correctly simulated.

Finally, the $1/C$ curve exhibits a strange behavior at low voltage, only visible when small voltage steps are used. Figure 3.5 shows this behavior, colloquially called a "foot," with a simulated $1/C$ curve and the extracted doping density. The large spike in the doping density profile is unreasonable. To prove this, I simulated the depletion of a diode with geometry identical to 2551-4-2. Figure 3.6 shows the comparison.

The foot in the C-V curve can be explained by looking at the non-uniformity of the surface of the detector due to the presence of the implants. The free electrons nearest to the implants will deplete first [6] with the process then continuing into the bulk of the

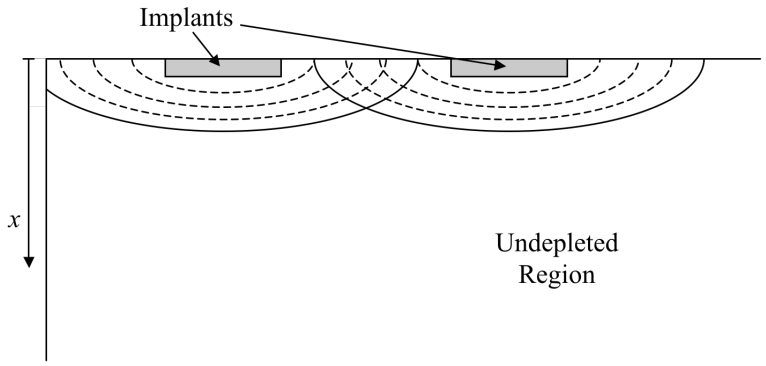

Figure 3.7: Depletion in the Region Between the Strips. The arcs surround the depleted area and increase in size as the voltage increases.

detector. Figure 3.7 shows an illustration of how the detector begins to deplete. As the voltage increases, the interface between the depleted region and the undepleted region will more closely resemble a plane, as in Figure 3.1.

To adjust the simulation to accommodate for this behavior, we need to omit the "foot" from our model because we do not know exactly what is happening in that region. This issue is unresolved but is beyond the scope of this paper, as well.

Evidently, this method isn't perfect, but it does provide a basic picture of the detector.

Chapter 4

Simulation Results

For this study, I made a number of comparisons between the doping density distributions and electric field profiles for various detectors. These results were obtained by simulating the depletion of the detector using the method described in Chapter 3.

4.1 Gamma Irradiation

Previous studies have shown that irradiating a detector with gamma rays increases its breakdown voltage [7]. This is because the photons cause radiation damage surface effects. Table 4.1 shows the gamma irradiated detectors I included in this study. The detectors were all irradiated with a ^{60}Co source in approximately 75 krad steps at a rate of 3.15 krad/hr. The detectors were not biased during irradiation.

The detectors were all fabricated by the SMART (Structures and Materials for Advanced Radiation Trackers) project using two different substrate materials: Float Zone (FZ) and Magnetic Czochralski (MCz). The detectors were also processed with two different levels of p-spray dose: high dose (5×10^{12} cm^{-2}) and low dose (3×10^{12} cm^{-2}) to isolate the n-type implants [8].

Table 4.1: Gamma Irradiated Detectors

Detector	Type	Substrate	P-spray Dose	Thickness (μm)
14-8	P	FZ	low	200
37-8	P	FZ	high	200
66-8	P	MCz	low	300
182-8	P	MCz	high	300

Figure 4.1 shows the effect of gamma radiation on detector 14-8 (p-type FZ with low p-spray). Figure 4.2 shows the simulated results for detector 37-8 (p-type FZ with high p-spray) after 76kRads and 304 kRads (pre-irradiation data was not included because it was unreliable due to the detector hitting breakdown before depletion). Both detectors showed a similar change as a result of being irradiated, with N_{eff} decreasing slightly throughout the bulk of the detector and the back side showing the largest effect.

In contrast, Figures 4.3 and 4.4 show the extracted doping density and electric field for two p-type MCz detectors, 66-8 and 182-8, respectively. For these SSDs, the effect of gamma irradiation seemed to be the opposite, with an overall increase in N_{eff}, especially at the back side.

Still, these results showed only minor changes in the effective doping density and surface effects near the strips could not be seen, due to the limitations of this simulation method.

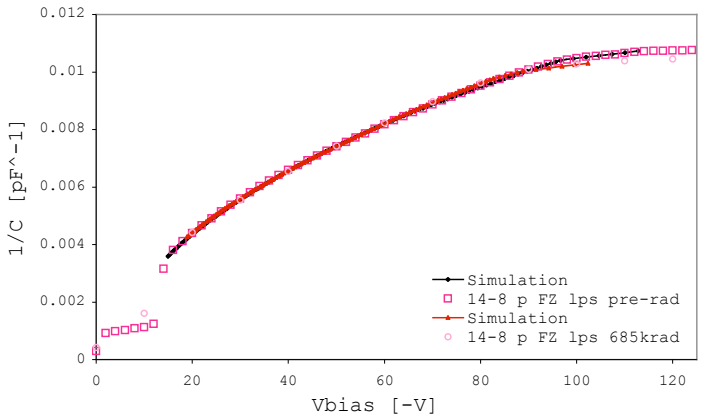

(a) $1/C$ vs. V_{bias} with Simulations

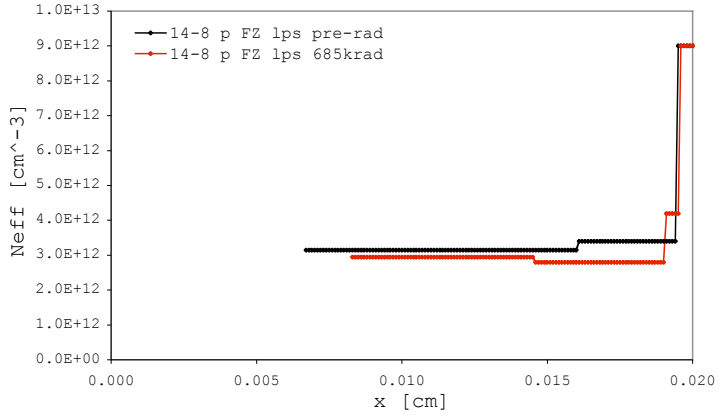

(b) Doping Density Distribution

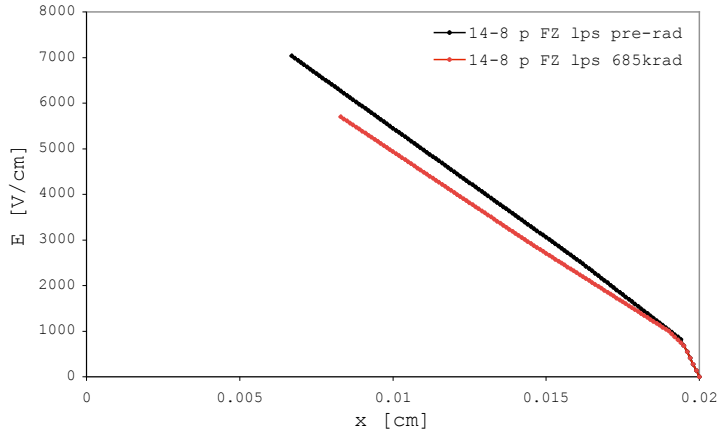

(c) Electric Field Profile

Figure 4.1: Simulated results for 14-8 (p-type FZ low p-spray dose) pre-rad and after 76kRads gamma irradiation.

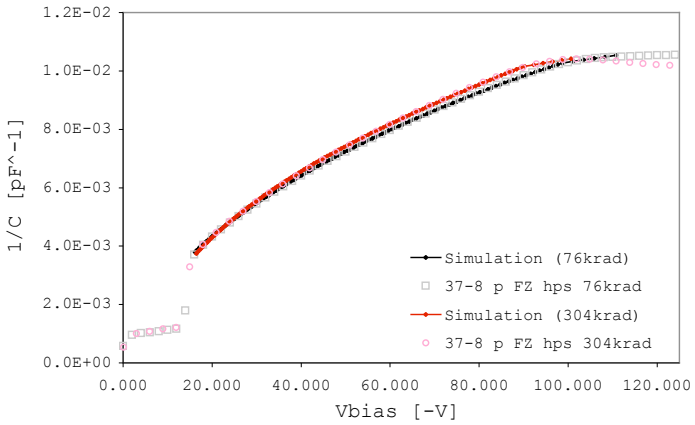

(a) $1/C$ vs. V_{bias} with Simulations

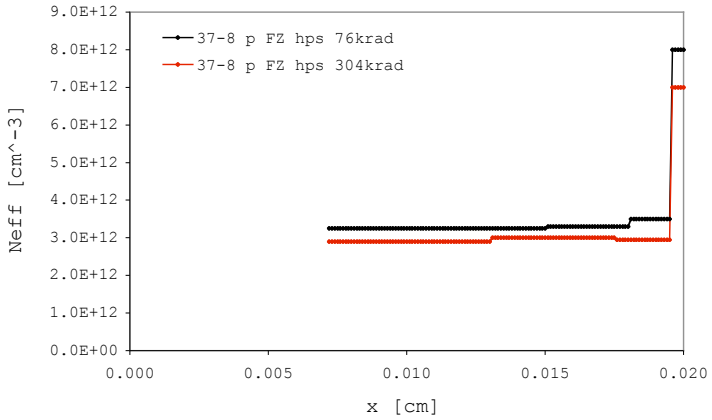

(b) Doping Density Distribution

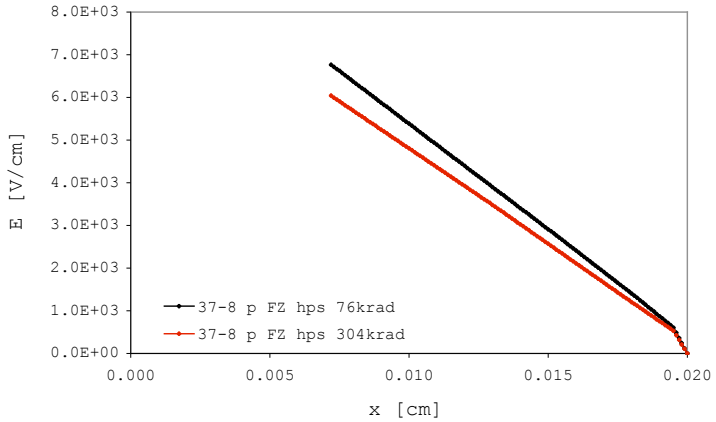

(c) Electric Field Profile

Figure 4.2: Simulated results for 37-8 (p-type FZ high p-spray) after 76 kRads and 304 kRads gamma irradiation.

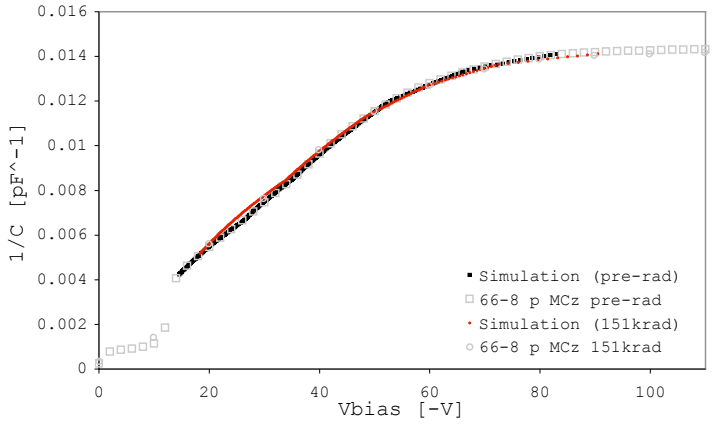

(a) $1/C$ vs. V_{bias} with Simulations

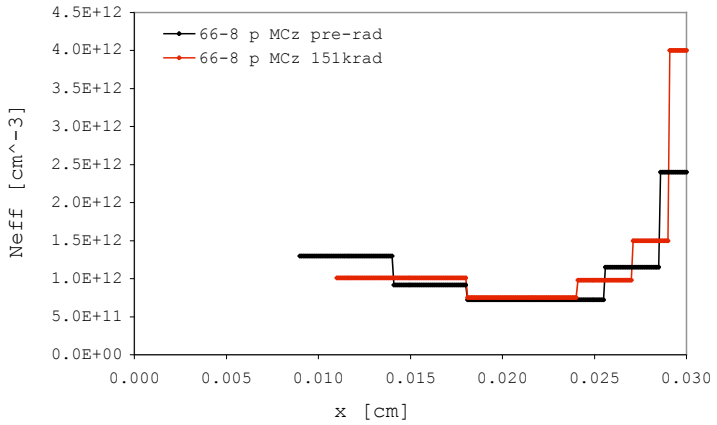

(b) Doping Density Distribution

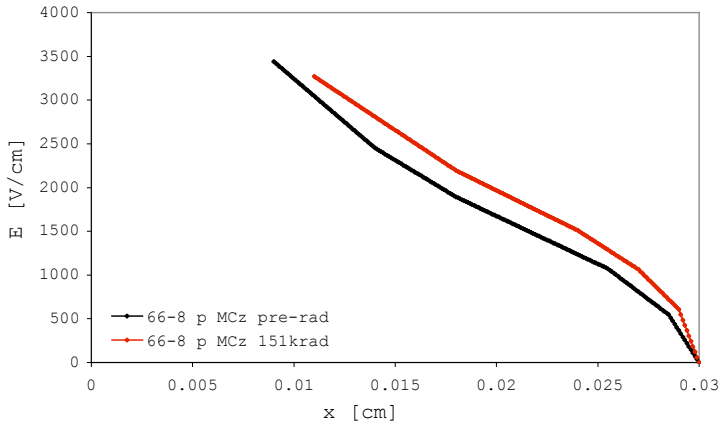

(c) Electric Field Profile

Figure 4.3: Simulated results for 66-8 (p-type MCz low p-spray) pre-rad and after 151 kRads gamma irradiation.

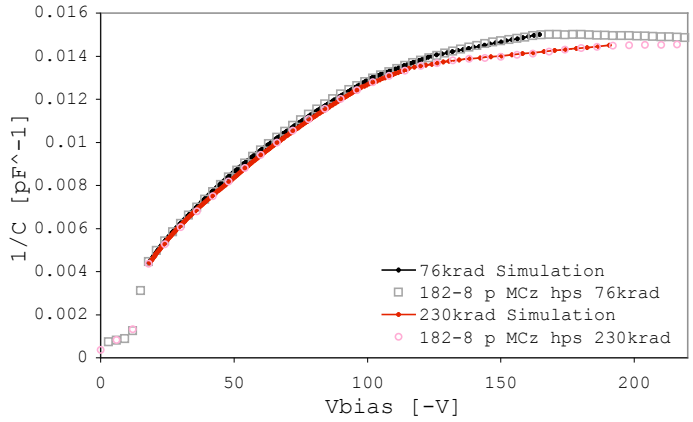

(a) $1/C$ vs. V_{bias} with Simulations

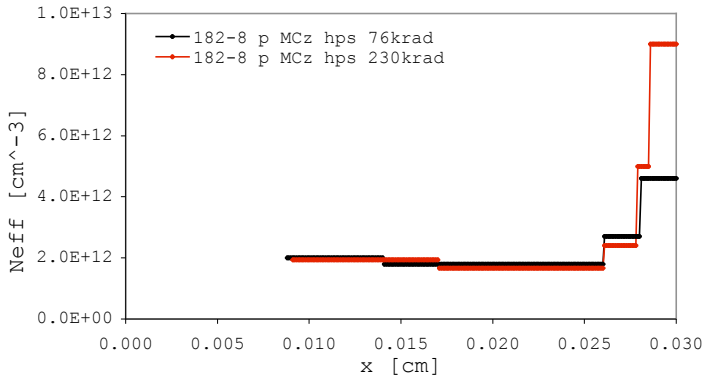

(b) Doping Density Distribution

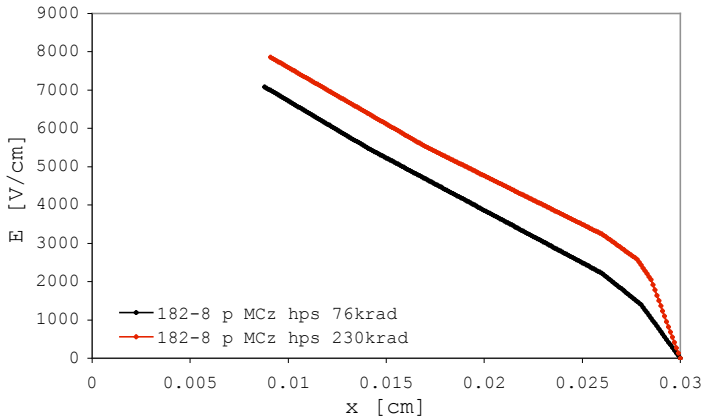

(c) Electric Field Profile

Figure 4.4: Simulated results for 182-8 (p-type MCz high p-spray) after 76kRads and 230 kRads gamma irradiation.

Table 4.2: Neutron Irradiated Detectors

Detector	Type	Substrate	P-spray Dose	Thickness (μm)	Fluence (neutron/cm^2)
14-5	P	FZ	low	200	4×10^{14}
1256-2	N	FZ	n/a	300	4×10^{14}
1256-3	N	FZ	n/a	300	(pre-rad only)
66-8	P	MCz	low	300	4×10^{14}
176-2	N	MCz	n/a	300	4×10^{14}
176-4	N	MCz	n/a	300	(pre-rad only)

4.2 Neutron Irradiation

Neutron irradiation has the effect of changing the doping density. According to previous studies, irradiation causes p-type doping to increase and n-type doping to decrease, so much so that n-type material can change to p-type after a high enough fluence (an effect called "type-inversion") [7]. To test this, I simulated the depletion for various detectors before and after different levels of irradiation. Table 4.2 lists the detectors I have included in this study and some of their properties.

All of the neutron irradiated detectors included in this study show essentially the same change after irradiation: a non-uniform increase in N_{eff} with the front and back sides experiencing the largest effect. The fact that wafer 176 (see Figure 4.8) did not show as large of an effect may suggest that at some point during the irradiation process it underwent type inversion, but because we don't have data at lower fluences, we can't say for certain.

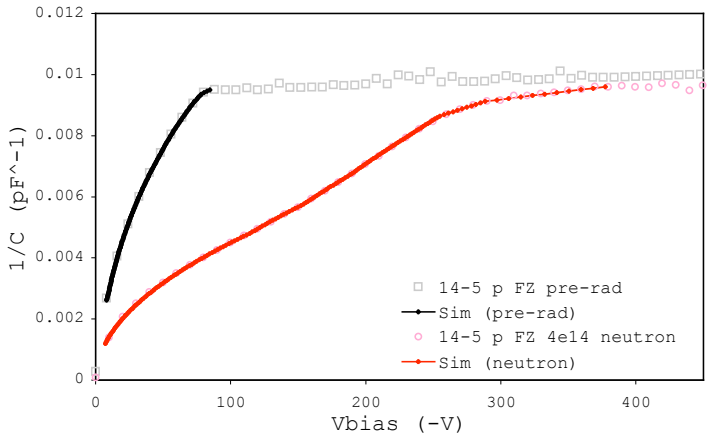

(a) $1/C$ vs. V_{bias} with Simulations

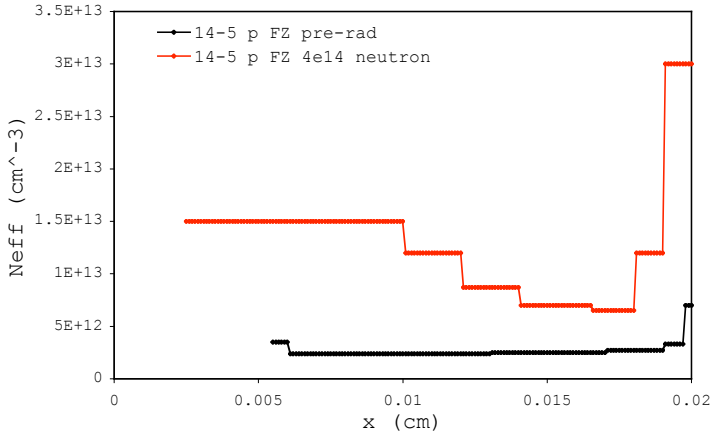

(b) Doping Density Distribution

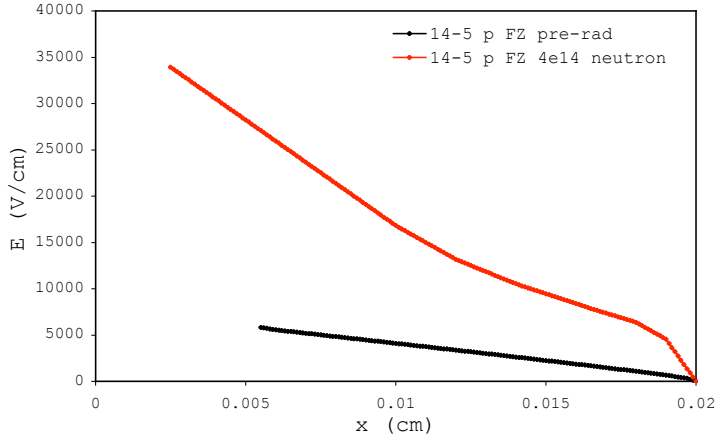

(c) Electric Field Profile

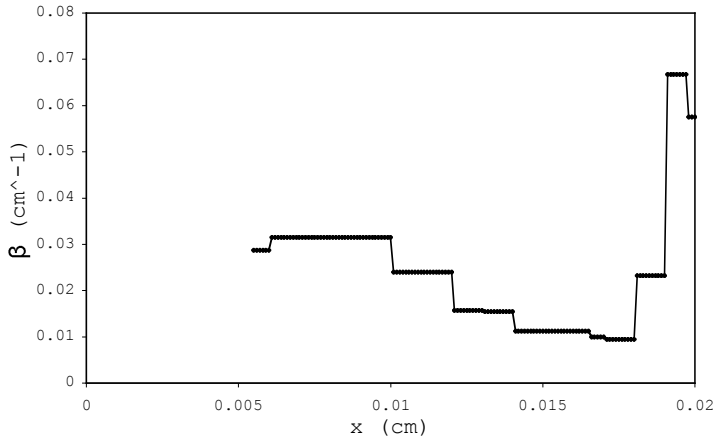

(d) $\beta(x) = \frac{\Delta N_{eff}(x)}{\Delta \phi}$

Figure 4.5: Simulated results for 14-5 (p-type FZ) showing effect of 4×10^{14} neutron/cm^2 irradiation.

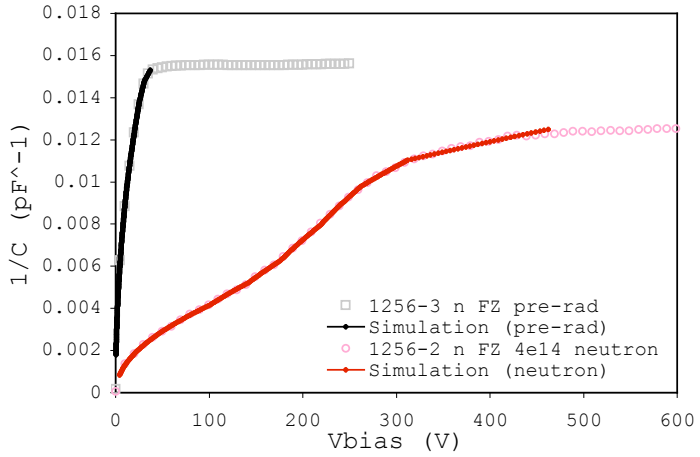

(a) $1/C$ vs. V_{bias} with Simulations

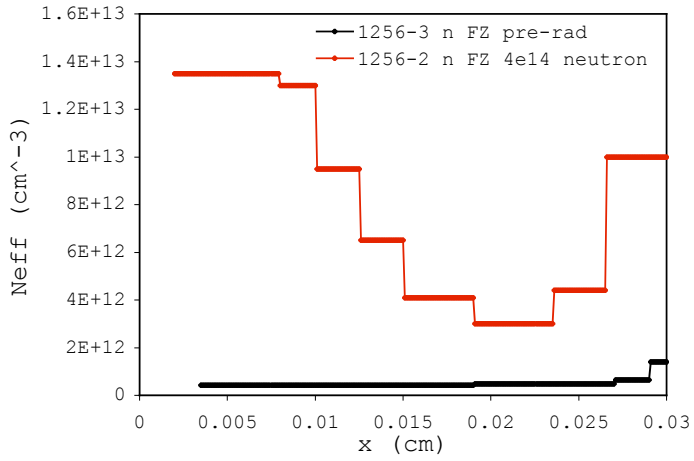

(b) Doping Density Distribution

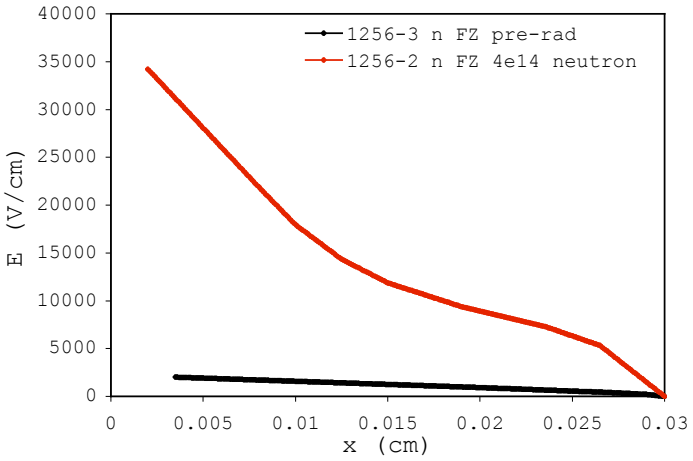

(c) Electric Field Profile

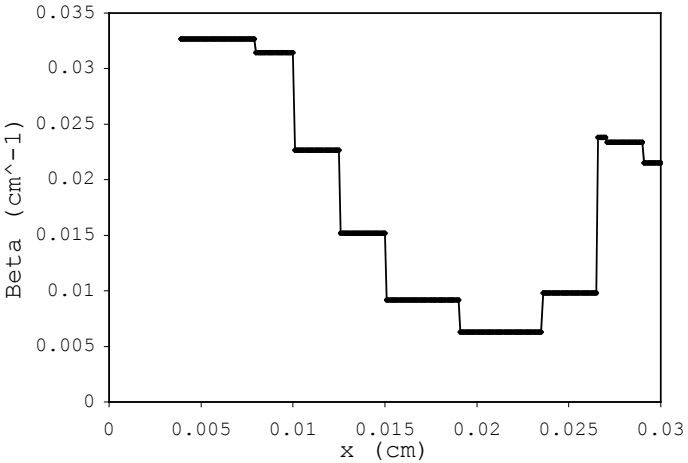

(d) $\beta(x) = \frac{\Delta N_{eff}(x)}{\Delta \phi}$

Figure 4.6: Simulated results for 1256-2 and 1256-3 (n-type FZ) showing effect of 4×10^{14} neutron/cm^2 irradiation.

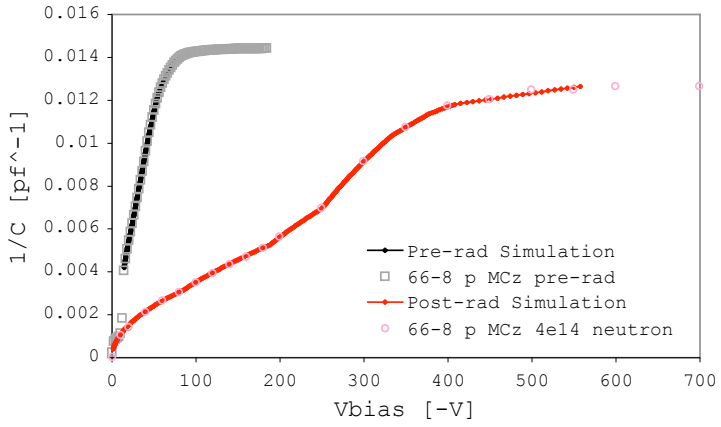

(a) $1/C$ vs. V_{bias} with Simulations

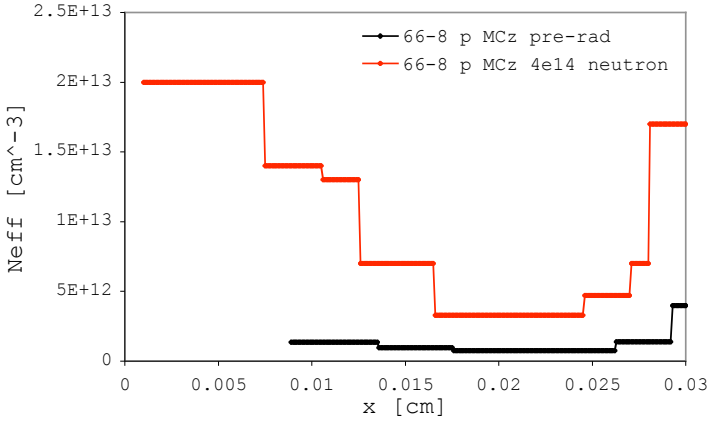

(b) Doping Density Distribution

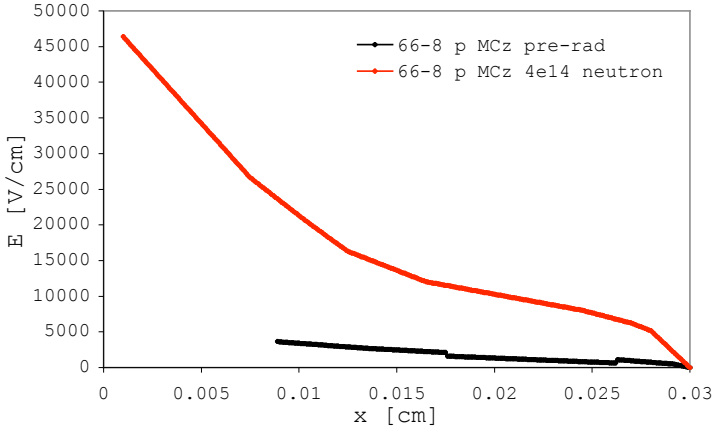

(c) Electric Field Profile

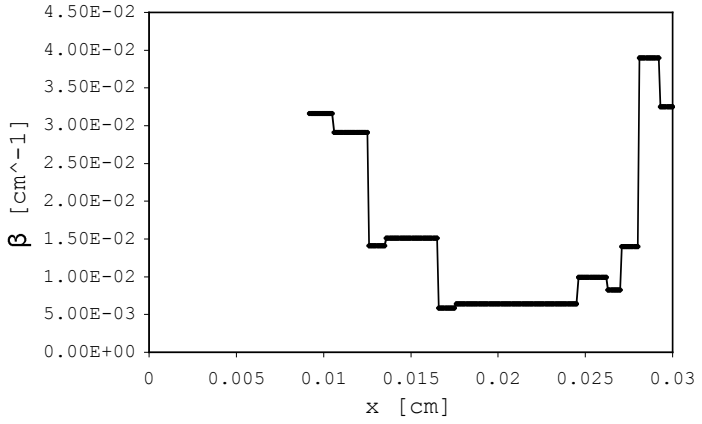

(d) $\beta(x) = \frac{\Delta N_{eff}(x)}{\Delta \phi}$

Figure 4.7: Simulated results for 66-8 (p-type MCz) showing effect of 4×10^{14} neutron/cm^2 irradiation.

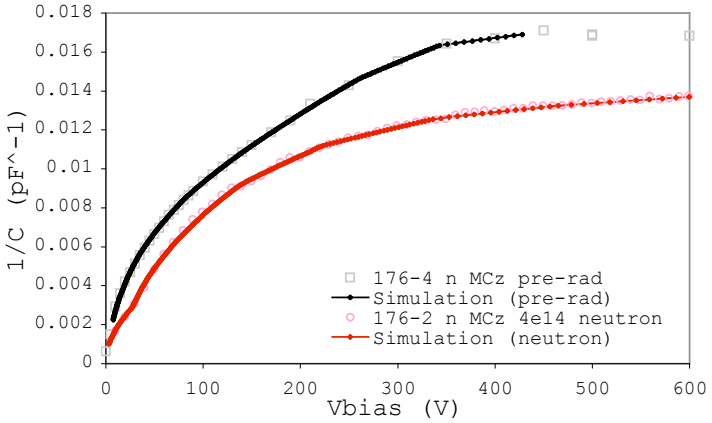

(a) Simulated $1/C$ vs. V_{bias}

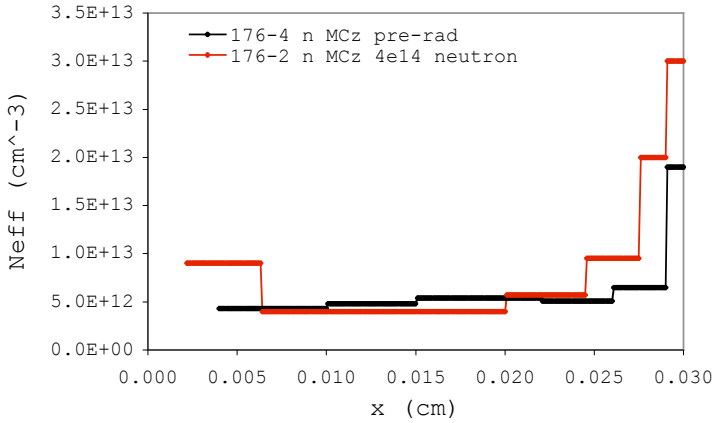

(b) $N_{eff}(x)$

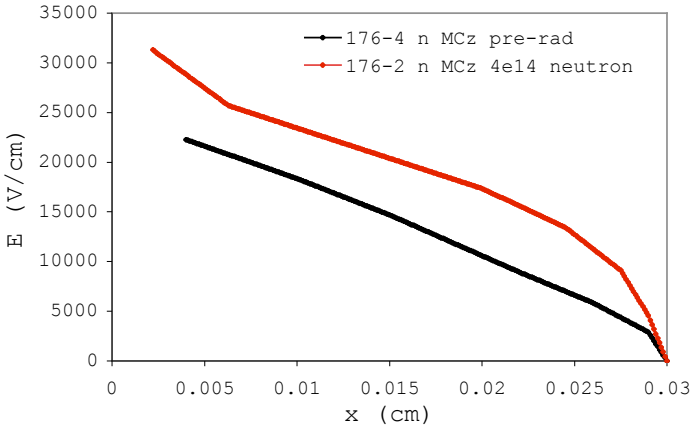

(c) Electric Field Profile

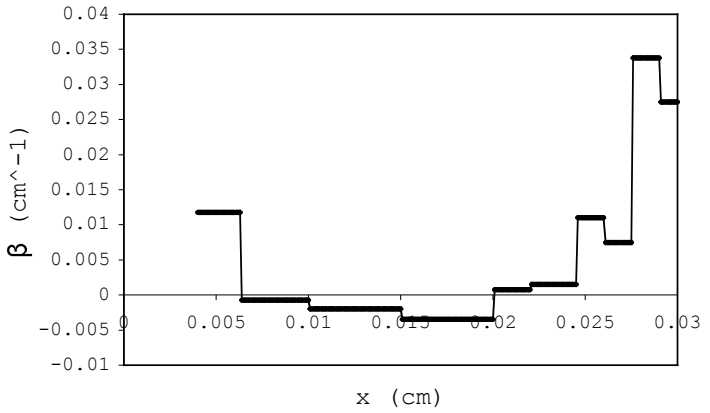

(d) $\beta(x) = \frac{\Delta N_{eff}(x)}{\Delta \phi}$

Figure 4.8: Simulated results for 176-2 and 176-4 (n-type MCz) showing effect of 4×10^{14} neutron/cm^2 irradiation.

Figure 4.9 shows the effective $\beta(x)$ and $N_{eff}(x)$ after irradiation for all four neutron irradiated detectors. From Figure 4.9a, it appears that neutron irradiation causes the largest change near the front and back sides, with the effect extending approximately 150 μm into the front and 50 μm into the back.

Figure 4.10 shows a comparison of C-V curves for the neutron irradiated detectors, showing that the scale of the effect was similar in all detectors except SSD 176.

The fact that the change in depletion voltage (V_{dep}) and N_{eff} was minor in detector 176 may suggest that it experienced type inversion. For an n-type detector, it is believed that V_{dep} and N_{eff} will (as a function of fluence) first decrease and then increase (after type-inversion) [3]. Because V_{dep} and N_{eff} were so high before irradiation and ended up at values only slightly higher suggests that we are simply seeing two points at very different points on a curve (see Figure 4.11 for a rough illustration of this).

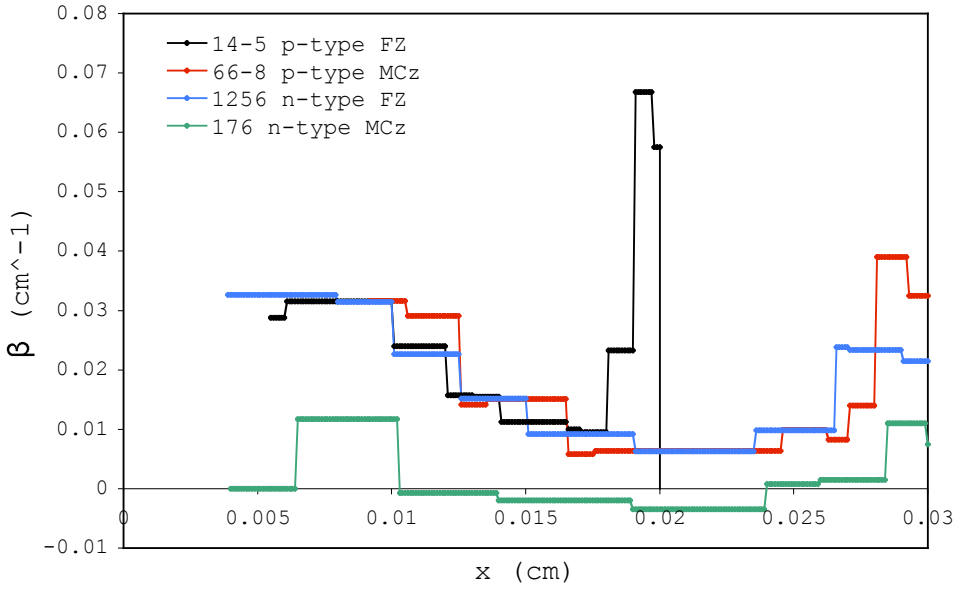

(a) Effective $\beta(x)$ comparison

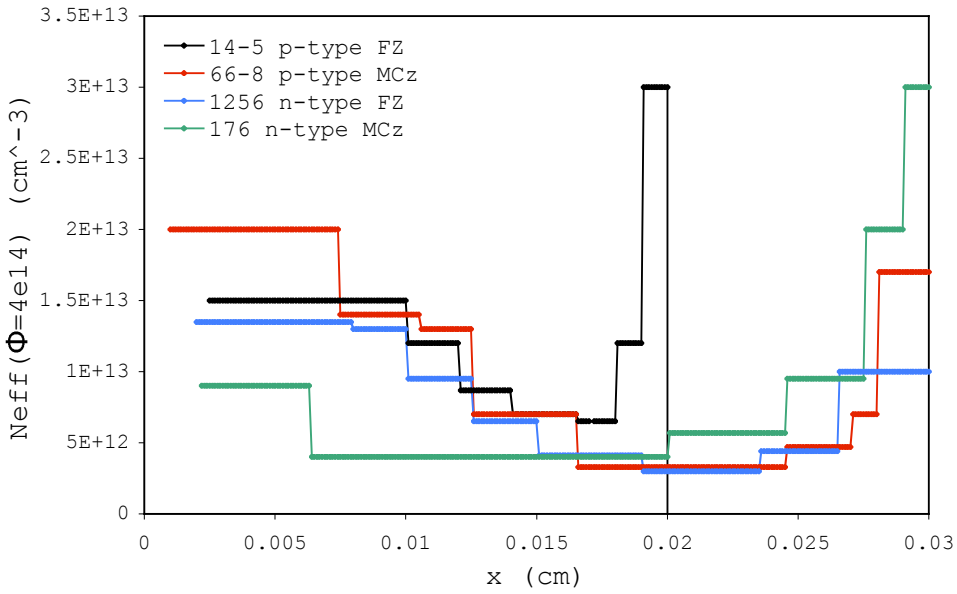

(b) Post-irradiation $N_{eff}(x)$ comparison

Figure 4.9: Effective $\beta(x)$ and $N_{eff}(x)$ after neutron irradiation. Note that SSD 14-5 is 200 μm thick while the others are 300 μm.

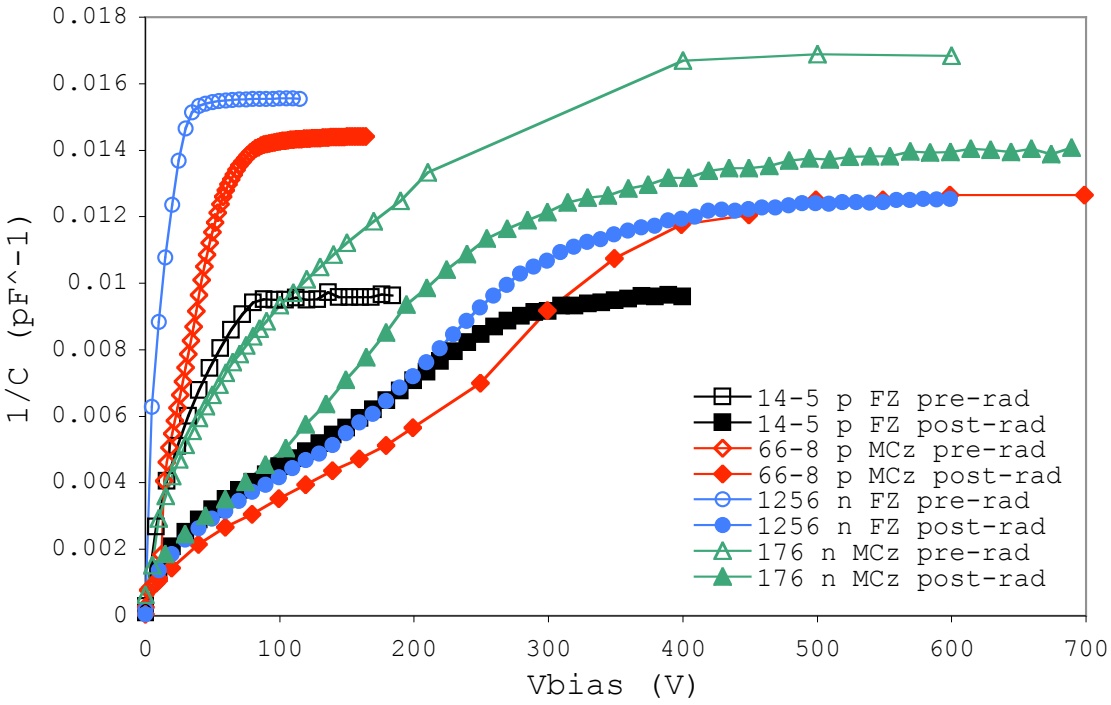

Figure 4.10: $1/C$ vs. V_{bias} comparison for neutron irradiated detectors.

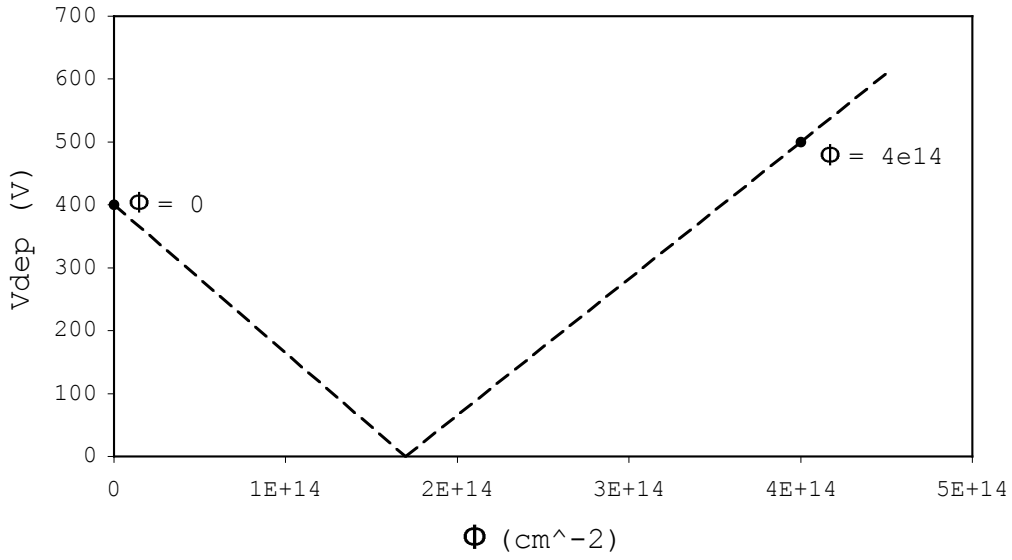

Figure 4.11: Mock-up illustration of what *may* have happened to V_{dep} as a function of ϕ for detector 176 (n-type MCz). The minimum of the curve may be the point at which type-inversion occurs, yet the only points we have data for are at $\phi = 0$ and 4×10^{14}. Note that it is unsure whether this curve should pass through zero or if it follows some other path.

Chapter 5

Conclusion

By simulating the depletion of various silicon strip detectors before and after irradiation, I was able to show the effect of gamma and neutron irradiation in a new way.

In developing this method and applying it to various detectors, a number of problems have become apparent:

- Because it only provides an approximation for the doping density distribution (N_{eff}), it fails to produce a continuous distribution.
- It does not accommodate for the possibility of a double junction after irradiation. Still, the model seems to produce good fits for the data, suggesting (but not proving) that the double junction is not yet seen at this fluence.
- It oversimplifies the detector, neglecting the complex region around the strips. In reality, the detector will deplete nearest to the strips first (as in Figure 3.7) and then continue uniformly into the bulk.

We are currently working to find solutions to these problems. Nonetheless, this method produces reasonable approximations for the doping density distribution and electric field

profile.

Using this method, I have shown that gamma irradiation causes only minor changes in the bulk of the detector, with the majority of the change seen at the back side. Both p-type Float Zone (FZ) detectors (low and high p-spray dose) showed a net decrease in doping density while both p-type Magnetic Czochralski (MCz) detectors showed a net increase in doping density.

I've also shown that neutron irradiation changes the detector dramatically, with the majority of the change seen at the front and back sides and very little change seen near the center of the detector bulk. This change was seen in both p and n-type FZ and MCz detectors. One detector tested (n-type MCz) saw little change in both doping density N_{eff} and depletion voltage V_{dep} after irradiation, possibly suggesting that it experienced type inversion.

Appendix A

Step by Step Procedure for Measuring C-V

A.1 Neutron Irradiated Detectors (Low Temperature)

1. Connect the Keithley HV supply and the Agilent LCR to the computer using GPIB cables. Connect the four terminal contact of the HP Test Fixture to the LCR. Connect the output of the Keithley to the input of the HP fixture. Connect two BNC cables to the outputs of the HP fixture.

2. Power on the computer, the Keithley, and the LCR.

3. Set the LCR to Cs-Rs (capacitor and resistor in series) mode and run open and short corrections.

4. Attach thermistor to the G10 immediately next to the detector. Use thermal grease to make good contact. Connect the thermistor to an ohmmeter. Verify that the resistance reads $\sim 108\Omega$.

5. Place the detector inside the styrofoam box and run the BNC cables through holes in the box. Connect the high potential output to the backside of the detector (G10) and the low potential to the bias ring (through the bond).

6. Feed the nitrogen hose into the side of the box and place lid on box. Plug all holes in the box loosely with foam to block out light. Cover with black cloth.

7. Open ADAP by typing `adap` at the command line. Choose the "Simple CV" template. Set the parameters in ADAP according to the detector you are testing. (See ADAP documentation for more details.)

8. Slowly add liquid nitrogen to the bottom of the container until the detector is at the desired temperature. Refer to Table A.1 for the resistance at various temperatures.

9. Click "Start Experiment" in ADAP. Continue to add nitrogen as needed to keep the temperature constant throughout the experiment.

Table A.1: Temperature vs. Resistance Table for Pt100 Thermistor

Temperature (degrees C)	Resistance (Ω)
20	108
10	104
0	100
-10	96
-20	92
-30	88

A.2 Unirradiated and Photon Irradiated Detectors (Room Temperature)

1. Connect the Keithley and the LCR to the computer using GPIB cables. Connect the four terminal contact of the HP Test Fixture to the LCR. Connect the output of the Keithley to the input of the HP fixture. Connect two BNC cables to the outputs of the HP fixture. Connect the BNC cables to probes.

2. Power on the computer, the Keithley, and the LCR.

3. Set the LCR to Cs-Rs (capacitor and resistor in series) mode and run open and short corrections.

4. Place the detector on a sheet of G10 and position it under the microscope.

5. Touch the probe connected to the high potential output to the G10 and the probe connected to low potential to the bias ring of the detector.

6. Close up the box to block out any light.

7. Open ADAP by typing `adap` at the command line. Choose the "Simple CV" template. Set the parameters in ADAP according to the detector you are testing. (See ADAP documentation for more details.)

8. Click "Start Experiment" in ADAP.

Bibliography

[1] "ATLAS Fact Sheet." <http://atlas.ch/pdf/atlas_factsheet_1.pdf>.

[2] M. Bruzzi. "Capacitance-Voltage analysis at different temperatures in heavily irradiated silicon detectors." SCIPP Preprint #06/12, 2006.

[3] A. Candelori. "Semiconductor Materials and Detectors for Future Very High Luminosity Colliders." IEEE Trans. Nucl. Sci. 52:6 (2005).

[4] I. W. Henderson. "Effects of γ-Irradiation on P-type Silicon Strip Detectors." B.S. Thesis. University of California, Santa Cruz, 2006.

[5] C. Betancourt, et al. "Expected Leakage Current for the ATLAS Upgrade Si Detectors." SCIPP Preprint #07/04, 2007.

[6] E. Barberis, et al. "Capacitances in silicon microstrip detectors." Nucl. Instr. and Meth. in Phys. Res. A 342 (1994) 90-95.

[7] D. M. Larson. "Pre-irradiation Capacitive Noise and Charge Collection Efficency of Silicon Strip Detectors." Master's Thesis. University of California, Santa Cruz, 2005.

[8] H. F.-W. Sadrozinski, et al. "Total Dose Dependence of Oxide Charge, Interstrip Capacitance and Breakdown Behavior of sLHC Prototype Silicon Strip Detectors and Test Structures of the SMART Collaboration." SCIPP Preprint #07/08, 2007.